

Halo Formation in Warm Dark Matter Models

Paul Bode*, Jeremiah P. Ostriker†

Princeton University Observatory, Princeton, NJ 08544-1001

and

Neil Turok‡

*DAMTP, Centre for Mathematical Sciences,
Wilberforce Road, Cambridge, CB3 0WA, U.K.*

(December 2, 2024)

Abstract

Discrepancies have emerged between the predictions of standard cold dark matter (CDM) theory and observations of clustering on sub-galactic scales. Warm dark matter (WDM) is a simple modification of CDM in which the dark matter particles have initial velocities due either to their having decoupled as thermal relics, or having been formed via non-equilibrium decay. We investigate the nonlinear gravitational clustering of WDM with a high resolution N body code, and identify a number of distinctive observational signatures. Relative to CDM, halo concentrations and core densities are lowered, core radii are increased, and large halos emerge with far fewer low mass satellites. The number of small halos is suppressed, and those present are formed by ‘top down’ fragmentation of caustics, as part of a ‘cosmic web’ connecting massive halos. Few small halos form outside this web. Small halos are typically found in regions of ten times higher density than those in CDM, where they are practically space-filling. If we identify small halos with dwarf galaxies, their number, spatial distribution, and formation epoch appear in better agreement with the observations for WDM than they are for CDM.

*email: bode@astro.princeton.edu

†email: jpo@astro.princeton.edu

‡email: N.G.Turok@damtp.cam.ac.uk

I. INTRODUCTION

Standard cold dark matter (CDM) theory appears to be in conflict with observations of clustering on sub-galactic scales. First, the theory predicts a very large number of low mass halos. For example, of order 500 satellites of mass greater than $10^8 M_\odot$ are expected within a halo as massive as that of the Milky Way whereas only 11 candidate dwarf galaxies with comparable mass are observed [1]. In the whole Local group, out to ~ 1.5 Mpc there are only 36 known dwarf galaxies [2], where several thousand would be expected in a straightforward interpretation of the theory. The second problem with CDM is that simulations produce halos with more concentrated cores than those inferred from the rotation curves of real galaxies [3]. There are a number of related but more complex problems. For example, the predicted satellites would lead to a thickening of the disks of galaxies which is not observed. And the dense cores, which form very early, would cause baryonic cooling to be too efficient, leading to disks with an order of magnitude too little angular momentum [4,5].

These problems may well have complex astrophysical solutions. Feedback processes such as heating and supernovae winds might inhibit star formation in low mass halos [6,7], although it is not clear why such processes would suppress the number of satellites without destroying them all. No convincing mechanism has been devised to explain the fact that most observed dwarf systems have characteristic densities which are considerably lower than those of dark matter halos of the same mass predicted from Λ CDM theory, and it certainly seems implausible that feedback processes would preferentially inhibit star formation in the denser halos. Further, dwarf spheroidals are believed to be completely dominated by dark matter, but their density profiles [8] show no sign of a central density cusp.

The situation regarding galaxy cores is as yet inconclusive. Improvements in rotation curve measurements [9] have brought the observations closer to the predictions of CDM, although a serious discrepancy remains if the typical density run at small radius is $\rho \propto r^{-1.5}$, as indicated in high resolution CDM simulations [3], [9], [10].

There is another potential problem with CDM, noted some time ago by Peebles [12]. The puzzle is that faint dwarf galaxies as measured in our vicinity (for a picture of the local $(8h^{-1} \text{ Mpc})^3$ volume see [13], p. 26) do not fill the voids in the bright galaxy distribution. Rather they tend to follow an even sharper distribution than the bright galaxies, tracing out surprisingly thin sheets around the voids. This effect has not as far as we know been systematically quantified, but is interesting in connection with the satellite problem of CDM. That is, observationally, dwarf galaxies seem both more strongly correlated with bright galaxies than in CDM, whilst at the same time being suppressed within large galaxy halos. In CDM theory both features are hard to understand, since the smaller halos formed earlier and should not be strongly correlated with later forming, larger scale structure. They should fill both the voids and massive structures alike, as we shall verify in our Λ CDM simulations presented below. Even if supernova winds or heating processes inhibit star formation in dwarf halos, and thereby suppress dwarf galaxies, it is hard to see why these processes would act preferentially in the voids. Another clue of potential significance is that observations [14] point to the formation of dwarf galaxies at $3 < Z < 4$, later than bright galaxies. This is not what one expects in a hierarchical theory like CDM where small objects should form first.

If these problems with CDM are real, they represent a remarkable opportunity. The

observed pattern of gravitational clustering may be revealing the physical properties of the dark matter. If so, this will be an invaluable clue to physics beyond the standard model. Deciphering this clue represents an exciting challenge in which both more refined observations and numerical simulations will be needed. Even if the conclusion of this work is that CDM theory survives, it will have been strengthened in the process. Alternative theories are valuable foils against which the successes of the better theory may be judged.

The small scale problems mentioned above do not negate the remarkable successes of the $\Omega_M \sim 0.3$, $\Omega_\Lambda \sim 0.7$ Λ CDM cosmology on larger scales [15]. These include the abundances and observed evolutionary properties of Lyman α clouds, large galaxies, clusters and of course the normalisation and shape of the power spectrum of cosmic microwave anisotropies. Therefore it seems sensible to seek a modest modification of the scenario whose sole effect is to damp small scale structure.

Free streaming due to thermal motion of particles, or Landau damping, is the simplest known mechanism for smearing out small scale structure. This process was central to the hot dark matter (massive neutrino) scenario for structure formation, which failed because the particle speeds were too high and erased perturbations up to tens of Megaparsec scales. Structure formation was ‘top down’, with galaxies forming only through fragmentation of pancakes, and at redshifts too low to be compatible with observation.

Warm dark matter (WDM) is just hot dark matter cooled down. We shall review below some of the many ideas in the literature as to how WDM might be produced. A particularly interesting possibility is that if the reheating temperature following inflation is low, then standard μ or τ neutrinos can be warm dark matter. Historically, WDM was considered (and quickly rejected) as a means of reconciling cluster abundances with a critical density for the dark matter [16]. That problem is resolved in the Λ CDM model by simply lowering the dark matter density. But the new problems faced by CDM motivate reconsideration of WDM (reincarnated now as Λ WDM) with a view to damping structure on sub-Megaparsec scales [4,17], requiring much lower particle velocities.

It is conventional to discuss WDM in terms of a canonical candidate, a light fermion with two spin degrees of freedom like the neutrino, assumed to decouple adiabatically and whilst still relativistic. The number of relativistic degrees of freedom at decoupling determines the effective temperature of the warm particles today, and the dark matter density determines the WDM particle mass m_X . We shall discuss WDM in terms of this mass, but it should be remembered that what really matters is the particle streaming speed, given for the canonical particle in equation (10) of the Appendix.

We discuss linear perturbation theory relevant to warm particles in the Appendix, where we derive the following formula for the smoothing scale, defined as the comoving half-wavelength of the mode for which the linear perturbation amplitude is suppressed by two:

$$R_S \approx 0.31 \left(\frac{\Omega_X}{.3} \right)^{.15} \left(\frac{h}{.65} \right)^{1.3} \left(\frac{\text{keV}}{m_X} \right)^{1.15} h^{-1} \text{Mpc.} \quad (1)$$

The scaling given here is different from that given in the previous literature on WDM (which mostly refers to [18] and [19]). The scaling usually given does not properly take into account streaming prior to matter-radiation equality.

The outline of this paper is as follows. In Section 2 we review particle physics mechanisms through which WDM may be formed. In Section 3, we discuss the lower bound imposed

on m_X by the requirement of early structure formation and in particular of reionising the universe (the Gunn-Peterson constraint). In Section 4 we discuss the phase space density (Tremaine-Gunn) constraint, and show that the initial thermal velocities of the particles are only relevant to the inner cores of halos, scales of hundreds of parsecs. The following sections are devoted to numerical results, revealing several potential observational signatures of warm dark matter.

We find that replacing cold with warm dark matter has the following effects:

1. Smoothing of massive halo cores, lowering core densities and increasing core radii.
2. Lowering greatly the characteristic density of low mass halos.
3. Reduction of the overall number of low mass halos.
4. Suppression of the number of low mass satellite halos in high mass halos.
5. Formation of low mass halos almost solely within caustic pancakes or ribbons connecting larger halos in a ‘cosmic web’. Voids in this web are almost empty of small halos, in contrast to the situation in CDM theory.
6. Late formation ($Z < 4$) of low mass halos, in a ‘top down’ process.
7. Suppression of halo formation at high redshift ($Z > 5$), and increased evolution of halos at lower redshifts relative to CDM.

The first four findings indicate that WDM holds some promise as a solution to the satellite and core density problems of CDM. The fifth is interesting as it may solve the problem raised by Peebles. The sixth and seventh items point to observational tests at high redshift, where there is the possibility of actually seeing the pancake formation as it first occurs. Recent HST observations probing galaxies at high redshift seem to indicate the formation of dwarf galaxies after bright galaxies [14], which is an argument in favour of WDM. It is perhaps worth emphasising that *WDM succeeds both in suppressing the number of satellites in large halos, whilst producing a distribution of dwarf halos in a cosmic web connecting higher mass galaxies*. All of these effects need to be better quantified in both observational data and simulations, so that precise statistical tests are possible.

It is a challenging problem at the limit of current numerical codes to simultaneously represent the modes responsible for structure formation (tens of Megaparsecs at least) whilst resolving objects as small as dwarf galaxies $< 10^8 M_\odot$. We chose the compromise of studying large boxes of $20h^{-1}$ Mpc with 256^3 particles in which we compare Λ CDM with Λ WDM, with WDM particle masses of $m_X = 175$ eV and 350 eV corresponding to smoothing scales R_S of 2.3 and $1.0 h^{-1}$ Mpc respectively. These values for m_X are almost certainly excluded by the Gunn-Peterson limit which we detail below, or by the limit from Lyman α clouds, pointing to $m_X > 750$ eV [20]. Nevertheless they are helpful for illustrating the qualitative differences between WDM and CDM clustering on large scales. We also performed a simulation with a more realistic value of $m_X = 1.5$ keV, corresponding to a smoothing scale of $0.19 h^{-1}$ Mpc, in smaller $3h^{-1}$ Mpc boxes with 128^3 particles. Finite size effects are important in this box, since long wavelength modes in the power spectrum are not properly represented. Nevertheless the simulation shows that the effects found at low m_X persist at higher values.

A second limitation is that with the current code, computation time becomes prohibitive for the 256^3 boxes at redshifts below unity. Therefore our largest simulations end at $Z = 1$. The signatures we identify deserve more detailed study, and larger simulations will be carried out in future work. Movies of the simulations were found to be very instructive in showing how structure formation in WDM proceeds. We have made these, higher resolution versions of the figures and some other results not included here available on the web, at <http://astro.Princeton.EDU/~bode/WDM/>.

Simulations have also been recently carried out by Colin, Avila-Reese & Valenzuela [21,22]. They found that WDM results in a reduction of the number of satellites in Milky-Way sized galactic halos, and in satellite halos with less centrally concentrated density profiles. The work presented here is in agreement with these findings. Moore et al. [3] simulated a $\sim 10^{12} M_\odot$ halo and found little difference in the density profile between warm and cold dark matter. White and Croft [23] used simulations to examine the nonlinear power spectrum in WDM models.

II. WARM DARK MATTER

In WDM, free streaming smears out perturbations on scales smaller than the comoving scale Δx over which a typical particle has traveled. In a flat FRW universe, the momentum p of a particle scales inversely with the scale factor a . This may be understood as a stretching of the de Broglie wavelength with a . The peculiar speed is given by the usual formula $v_p = p/\sqrt{p^2 + m_X^2}$, with $p = m_X a_{nr}/a$, where a_{nr} is the scale factor when the particle becomes non-relativistic (i.e. when $v_p = c/\sqrt{2}$). The motion in comoving coordinates is given by $dx/dt = v_p/a \approx c a_{nr} a^{-2}$ at late times. In the matter era, where $a \propto t^{\frac{2}{3}}$, the comoving displacement Δx converges. A crude estimate of the smoothing length is obtained by multiplying the speed of the particle at matter-radiation equality by the comoving horizon scale at that time. Up to a numerical factor this is the smoothing scale usually quoted [18], [19];

$$R_{>eq} \approx 0.2 (\Omega_X h^2)^{\frac{1}{3}} \left(\frac{1.5}{g_x} \right)^{\frac{1}{3}} \left(\frac{\text{keV}}{m_X} \right)^{\frac{4}{3}} \text{Mpc.} \quad (2)$$

However the situation is actually more complicated since for the warm particle speeds of interest the particles become nonrelativistic long before matter-radiation equality. There is thus a substantial period of time in the radiation era during which the Jeans mass is low and linear perturbations grow logarithmically with time, whilst the comoving displacement is also growing logarithmically (since $a \propto t^{\frac{1}{2}}$ in the radiation era). The linear evolution of perturbations during this epoch may be understood using the nonrelativistic Gilbert equation discussed in the Appendix, which leads to the improved scaling formula given in (1) above, and which we used in the simulations described below. But for a crude discussion, as we give now, the the scaling of the smoothing length (2) is certainly adequate.

Warm dark matter is most simply discussed in comparison with the usual hot dark matter scenario. In the discussion which follows we shall generally choose cosmological parameters $\Omega_{DM} = 0.3$ and $h = 0.65$, unless otherwise stated. In the hot dark matter scenario (with a single massive neutrino) the particle mass would be 12 eV. These neutrinos would have

thermal speeds of $v_s/c \sim 0.2$ at equality, and their motion would erase structure on comoving scales of ~ 25 Mpc. If we wish to preserve the successes of CDM theory on comoving scales greater than say 0.1 Mpc, we need to reduce the streaming speed by a factor of 250.

For a thermal relic particle which is relativistic at decoupling but nonrelativistic by equality, the typical streaming speed at equality is $v_s/c \propto T_X/m_X$, where T_X is an effective temperature varying inversely with the scale factor. Neglecting the subtleties of logarithmic growth in the radiation era, this speed determines the streaming length. To lower v_s by 250 we need to either lower T_X or raise m_X . However, if the particle decouples with thermal abundance, then we have $\rho_X \propto T_X^3 m_X$ which must be held fixed to explain the dark matter today. Thus to obtain the desired reduction in v_s we must lower T_X by ~ 4 and increase m_X by $\sim 4^3 = 64$, bringing it close to 1 keV.

The factor of ~ 4 reduction in T_X could be produced in several ways. The simplest is that the X particles decoupled when there were 64 times the number of relativistic degrees of freedom than when neutrinos decoupled, i.e. $64 \times 10.75 = 688$. This requires several times more degrees of freedom than present in the standard model (106.75) or supersymmetric versions (~ 200). A substantially larger number is certainly possible in theories with larger gauge groups and representations, especially those with extra dimensions. As far as we know, no detailed computations of entropy release have been performed in the latter case, but at temperatures above 1 TeV the large number of Kaluza-Klein modes would surely become important. If the dark matter particle possesses only gravitational strength couplings and therefore decouples early, it would be left with a substantially lower effective temperature than the radiation fluid. A plausible candidate would be the gravitino [24].

In fact, all that is really required is that there be some release of entropy after X decoupling. One possibility is that the universe became dominated by some form of matter with $P < \frac{1}{3}\rho$ after X decoupling. For example, a mild first order phase transition with some supercooling and latent heat release, a rolling scalar field which dominated briefly before being converted to radiation, or a massive species which dominated before decaying into radiation but not X 's. This must happen when the temperature was greater than ~ 1 MeV if it is not to disturb nucleosynthesis.

Another apparently viable scenario, discussed recently [25], [26] is that the reheating temperature after inflation T_{RH} was low, so that the maximum temperature of the radiation era was in fact only a few MeV. In this case, if the neutrinos are only produced via electron positron annihilation, their number density can be considerably lower than in the usual equilibrium scenario. As ref. [25] points out, although this reduces the expansion rate of the universe which decreases the helium abundance, there is a compensating effect because there are fewer neutrinos to convert neutrons to protons. According to [26], in such a scenario, ordinary neutrinos may be resurrected as warm dark matter. Reference [26] gives $\Omega_\nu h^2 = (m_\nu/70 \text{ keV})(T_{RH}/\text{MeV})^3$ for the density of μ and τ neutrinos where m_ν is the neutrino mass [27]. Recalling that the desired momentum (in units where $c = 1$) is $\sim 10^{-3}m_\nu$ at equal density, it is $\sim 10^3 m_\nu T_{RH}/\text{MeV}$ when the neutrinos are produced. The neutrinos are radiated from electron-positron and neutrino-antineutrino pairs in the hot plasma with thermal momenta $p \sim 3T_{RH}$ assuming $T_{RH} \gg m_\nu$. These equations imply $m_\nu \sim 3$ keV, and for $\Omega_\nu \sim .3$ and $h \sim 0.65$ we obtain $T_{RH} \sim 2$ MeV. The numerical coincidence here is very interesting, and deserves further study. Note also that in this scenario, the number densities of μ and τ neutrinos are suppressed, so that matter-radiation equality is now at

a higher redshift (by about thirty per cent). This is helpful in that there is more time for structure to form, alleviating the reionisation bound discussed below. Interestingly, it also shifts the Doppler peak of the CMB anisotropy to lower l .

A different alternative is that X particles carry a conserved charge like baryon number, and an X asymmetry is formed as a result of non-equilibrium CP violating processes. In this case we would have (as for baryons) $\rho_X \sim \epsilon m_X T_X^3$ with ϵ a dimensionless CP violating coupling. Assuming the dark matter particles have the same temperature as neutrinos, slowing them down by the required amount would require their mass be increased by 250, thus we would have $m_X \sim 3$ keV, and the required dark matter density is attained for $\epsilon \sim .004$.

One may also consider X particles produced via entirely non-thermal mechanisms. One idea [28] is that a supersymmetric condensate simultaneously decays into the lightest super-particles, which form the dark matter, and baryons, in a ratio which explains the observed coincidence in their densities today. If the condensate mass were of order 300 times the dark matter particle mass, and if the decay took place at around 1 MeV, then the dark matter particles would have gamma factors of $p/m_X \sim 300$ at that time, and speeds of $3 \times 10^{-4}c$ at matter-radiation equality, equivalent to a 1 keV warm particle.

Other examples of non equilibrium production of warm particles are resonant production of sterile neutrinos via oscillation from active neutrinos [29], and particle production from the decay of massive particles or cosmic defects [30].

Even from this limited discussion it is clear that there is an (over) abundance of mechanisms for producing warm dark matter, using modest extensions of physics beyond the standard model.

III. EARLY STRUCTURE FORMATION IN WDM

If one uses WDM to solve CDM's small scale problems there is a window of allowed streaming speeds: too low and the WDM is just like CDM; too high and structure formation begins too late, as in HDM. A particularly stringent limit is the Gunn-Peterson bound [31], provided by the fact that quasar spectra reveal little absorption from smoothly distributed atomic hydrogen. Thus the intervening regions of the universe must have been almost completely ionised. The highest redshift quasars (at $Z = 5.5$ and 5.8) have only recently been discovered [40,41], and have normal spectra. There must therefore have been enough UV radiation released from stars or AGN to fully ionise the universe by this epoch [31].

The fraction of the baryons which could plausibly have undergone gravitational collapse and star formation by a given redshift is easily computed (assuming the primordial fluctuations are Gaussian) from the power spectrum given in the Appendix. The fraction of the universe f_{nl} attaining an overdensity greater than δ_c at some redshift is just probability that $\delta > \delta_c$ at any one point. We choose δ_c to be the linear theory amplitude corresponding to collapse to zero radius in the nonlinear spherical collapse model. In an $\Omega_M = 0.3$ flat cosmology, one has $\delta_c \approx 1.675$ [32], slightly smaller than the canonical critical density value of 1.69. We compute the fraction f_{nl} by integrating the power spectrum and employing the linear theory growth factor appropriate to this cosmology. The result for f_{nl} at redshifts 7, 6, 5, 4, 3 is plotted as the solid curves in Figure (1) as a function of the warm particle mass, assuming the canonical neutrino-like particle and a Λ WDM theory normalised to COBE ($\sigma_8 = 0.9$).

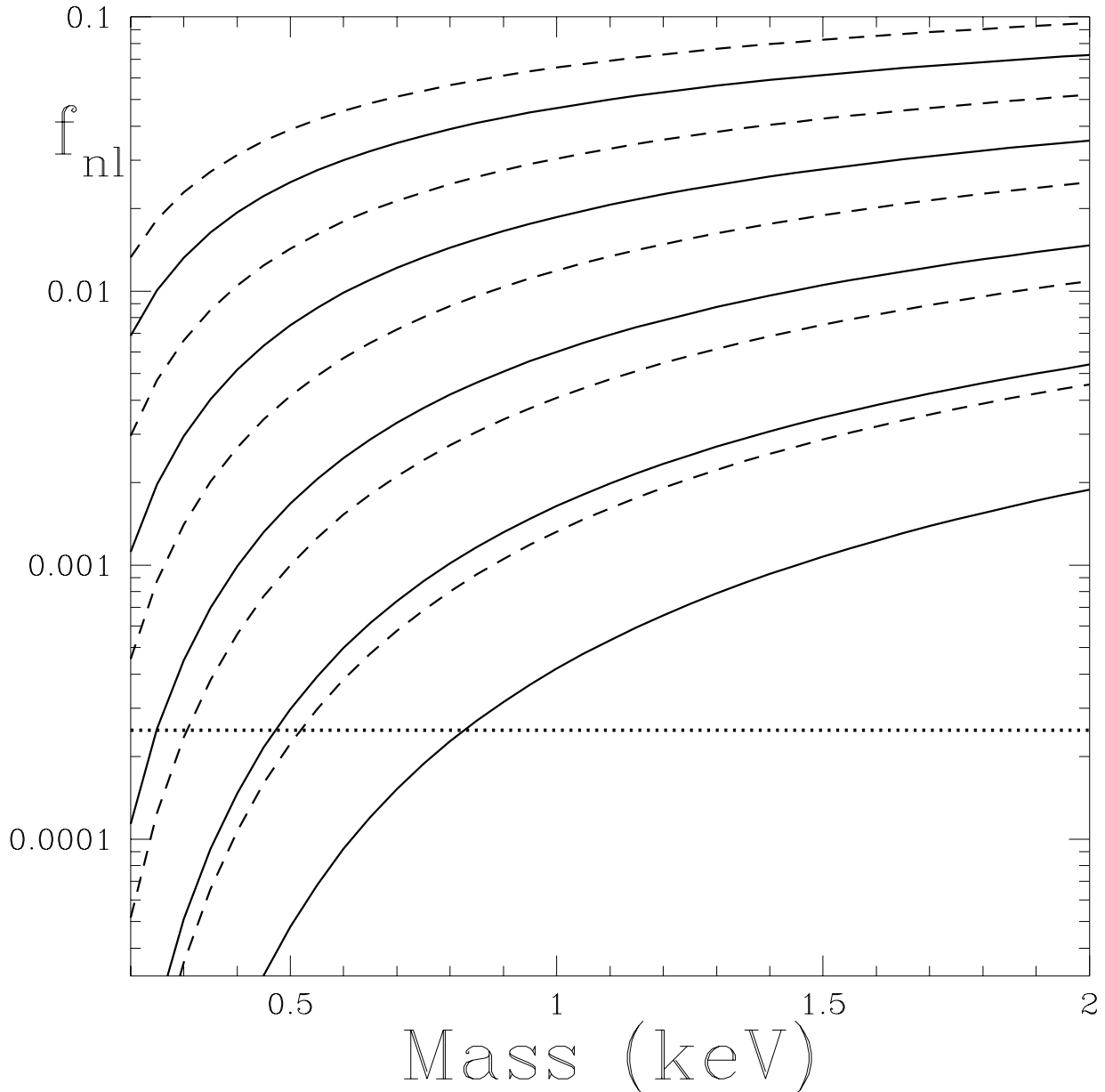


FIG. 1. The collapsed fraction f_{nl} , defined to be the fraction of matter in the universe which has attained a linear theory perturbation amplitude corresponding to collapse to zero radius in the spherical collapse model. The fraction f_{nl} is plotted at redshifts 7, 6, 5, 4, 3 (lower to upper curves) for warm particle masses from 0.2 to 2 keV. The solid curves are for the theory normalised to $\sigma_8 = 0.9$ and the dashed curves for $\sigma_8 = 1.0$. The horizontal line shows an estimate of the fraction of mass which must be collapsed in order to re-ionise the universe. This is based on an assumed stellar population similar to that observed today. In addition a factor ~ 3 should be included to account for inefficient propagation and for recombination. The observation of a quasar at $Z = 5.8$ whose spectrum exhibits little absorption due to neutral hydrogen sets a lower limit on the mass of the warm particle, $m_X \lesssim 400 - 700$ eV for this estimate. Cosmological parameters $\Omega_M = 0.3$, $\Omega_\Lambda = 0.7$ and $h = 0.65$ are assumed.

When baryons are bound into stars, nuclear burning releases on order 4 MeV per baryon. To ionise hydrogen, 13.6 eV is needed, thus a conservative bound is that at least 3.4×10^{-6} of the universe must have undergone gravitational collapse in order to re-ionise the universe. (Even this limit is not completely watertight, since black holes can release more energy per gram than stars). A more realistic bound is obtained by assuming that the first generation of stars was typical of star forming regions today: for such a population nuclear burning releases on order 4000 ionising photons per baryon [37]. This leads to a bound $f_{nl} > 2.5 \times 10^{-4}$. A greater nonlinear fraction is needed if one allows for recombination in denser clumps. Gnedin and Ostriker [33] find (for Λ CDM) that 10 photons above 13.5eV are required for each net ionisation. Note however that a WDM universe is very smooth at early times between the high peaks, so clumping is likely to be less significant than in CDM [37].

The fraction f_{nl} is very sensitive to the value of σ_8 since the latter occurs squared in the exponent of the Gaussian probability distribution. In Figure 1 we show the results of increasing σ_8 from 0.9 (the result for a COBE-normalised $n = 1$ primordial spectrum) to $\sigma_8 = 1.0$. The latter would be appropriate for COBE normalisation with a small positive tilt, $\delta n \sim 0.02$. At present such a tilt cannot be ruled out, although future CMB data may eventually allow one to do so. Figure 1 shows that a minimal warm mass of order 400 eV (700 eV) is needed for $\sigma_8 = 1.0$ (0.9), if one allows an additional factor of 3 for recombination. A more detailed treatment of the reionization limit leads to the requirement $m_X \gtrsim 1.5\text{keV}$ [34].

The way in which structure forms in WDM is conveniently illustrated in Figure 2. This shows the rms mass fluctuation σ_M in linear theory, computed in a spherical top hat window of varying radius, plotted against the comoving mass contained in the window. It is given in units of the linear theory growth factor $g(Z)$, normalised to unity at $Z = 0$. At $Z = 1, 2, 3, 4, 5, 6, 7$, one obtains $g(Z) = 0.61, 0.42, 0.32, 0.26, 0.21, 0.18, 0.16$, slightly higher than the standard critical density result $g(Z) = (1 + Z)^{-1}$.

Above the WDM smoothing scale the theory behaves like CDM. But as the mass scale is lowered, the rms mass fluctuation tends to a constant, just because the density field is smooth on small scales. Gravitational collapse occurs in most of the mass in objects whose scale is of order the WDM smoothing scale. These objects collapse when the linear theory rms amplitude σ_M reaches of order unity. From Figure 2 and the values of $g(Z)$ given above we see that the corresponding redshift increases roughly from 3 to 5 to 7 as the warm particle mass is increased from 0.5 to 1.5 to 3 keV. So in WDM one expects to see a great deal more evolution of galaxy scale objects at these redshifts than in CDM.

What about the formation of dense collapsed objects like the centres of bright galaxies? In the simplest treatment, using the spherical collapse model, these regions have an overdensity of ~ 200 at the moment of collapse and thereafter their overdensity scales as $(1 + Z)^3$. Thus halos collapsing at redshifts ~ 4 could plausibly attain overdensities of a few times 10^4 today. This is within an order of magnitude of the observed overdensities of the inner parts ($r < 10h^{-1}$ kpc) of bright galaxies as inferred from rotation curves ($v_{rot} \sim 200 \text{ km s}^{-1}$ implies an overdensity of $\sim 3 \times 10^5$). Since these regions contain a mass of $\sim 10^{11}h^{-1}M_\odot$, and the number density of such galaxies is $\sim 10^{-2} h^3 \text{ Mpc}^{-3}$, for $\Omega_M \sim 0.3$ they constitute around 1 per cent of the mass in the universe. From Figure 1, we see that for warm particle masses greater than 700 eV, and with $\sigma_8 = 0.9$, more than one per cent of the dark matter collapsed by redshift 4. But as we lower the mass, the curves steepen and the corresponding

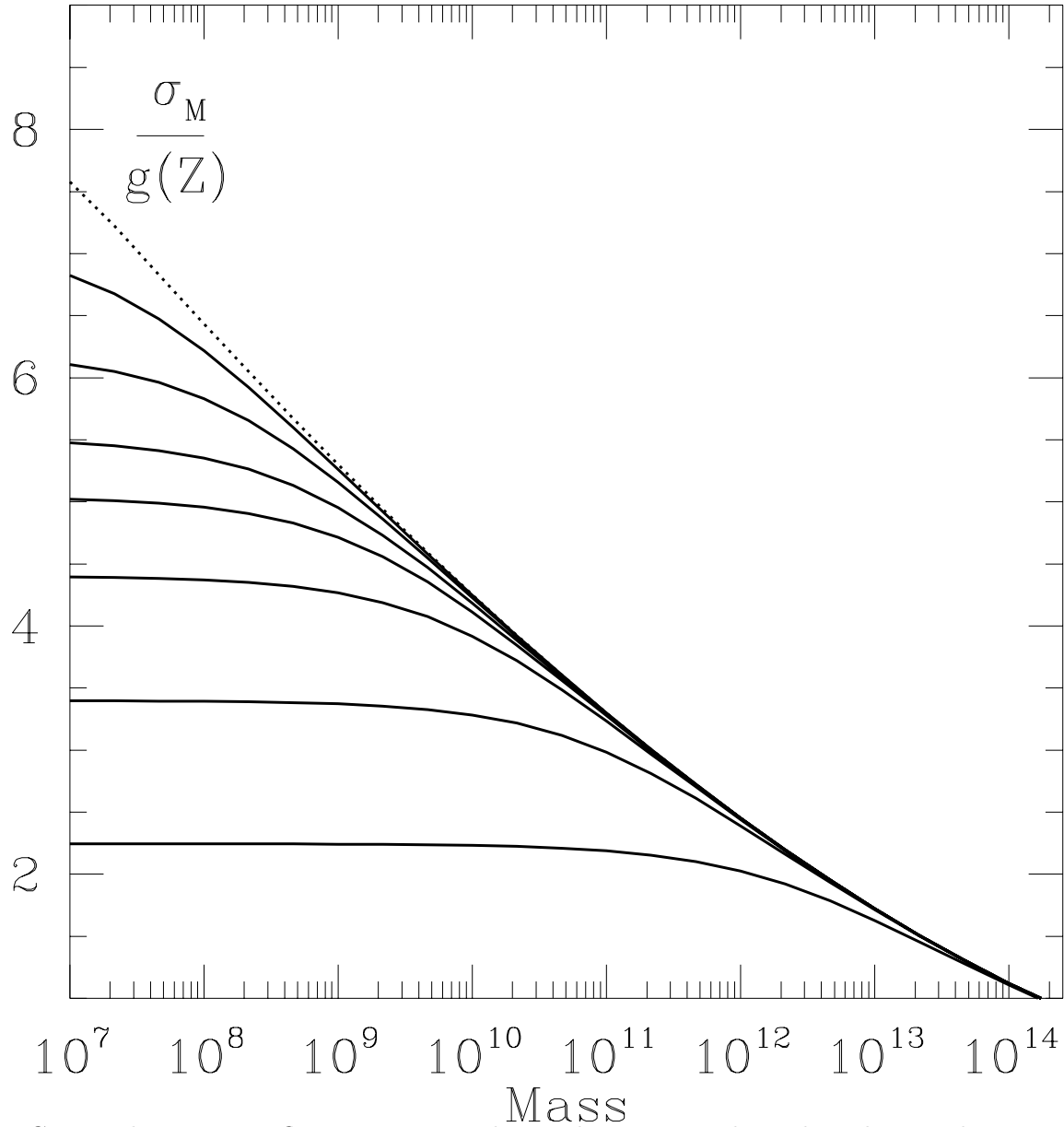


FIG. 2. The rms mass fluctuation σ_M in linear theory, in a spherical top hat window, given in units of the linear theory growth factor $g(Z)$ which is normalised to unity today. The solid lines show σ_M against the comoving mass in the window for WDM particle masses of 0.2, 0.5, 1.0, 1.5, 2.0, 3.0 and 5.0 keV (bottom to top). The theories are normalised to $\sigma_8 = 0.9$, consistent with an assumed $n = 1$ primordial spectrum and the COBE results. The dotted line shows the same quantity $\sigma_M/g(Z)$ for CDM. Cosmological parameters $\Omega_M = 0.3$, $\Omega_\Lambda = 0.7$ and $h = 0.65$ are assumed.

redshift falls steeply. Thus it is clear that warm particle masses lower than ~ 500 eV are strongly constrained by the requirement that dark matter halos with the observed properties are formed.

What about smaller objects? Dwarf galaxies, like Draco and Ursa Minor have half masses of $\sim 1.0 \times 10^7 M_\odot$ and half mass radii of ~ 500 pc [35]. This corresponds to a characteristic density of $2 \times 10^{16} M_\odot/\text{Mpc}^3$ and an overdensity of 5×10^5 for currently favoured cosmologies; they are believed to be dominated by dark matter. They also have very low line of sight velocity dispersions, $\sigma \sim 9 \text{ km s}^{-1}$ [2]. Small objects like this are only formed in WDM through fragmentation of caustics at late times in the vicinity of larger mass galaxies. As we discuss in the next section, their densities are perfectly compatible with the Gunn-Tremaine bound (which yields a mass limit $m_X > 400$ eV for the canonical warm candidate). But how can such cold, relatively dense objects ever form? The most plausible location is at the centre of caustics. For cold planar collapse, the density of the virialised sheet diverges as the normal distance z tends to zero, as $z^{-\frac{1}{2}}$ [13]. If a particle turns around at coordinate z at time t_c its peculiar velocity is $\sim z/t_c$. Let us assume that t_c is the time corresponding to $Z = 4$, $t_c \sim 0.11 H_0^{-1}$ for Λ WDM with $\Omega_M = 0.3$. Then if z is the comoving scale corresponding to the mass of a dwarf, $d \sim 0.07/(1+Z) \sim .01$ Mpc, we find a collapse velocity of $\sim 6.5 \text{ km s}^{-1}$, similar to what is observed. Clearly this issue requires further study, but the estimate is not discouraging.

It is interesting to compare inferred dark halo overdensities over the full observational range, from dwarf galaxies to rich clusters of galaxies. The latter constitute a mass fraction of order a few per cent to the universe; $\sim 10^3$ halos of $\sim 10^7 M_\odot$ comprise a similar fraction of the mass of a giant halo. Assuming the latter provides a fair sample of the universe, dwarf halos form from density peaks of comparable rarity to those which form giant clusters. As an example of a well studied cluster, see [36]. The mass is $\sim 10^{15} h^{-1} M_\odot$, and the inferred half-mass overdensity is 2.5×10^3 in this cosmology. (Here we are being conservative, in including the entire infall mass outside the virial radius.) The usual scaling argument applied to hierarchical structure formation (e.g. [13], p. 628) predicts that the overdensity for collapsed halos $\rho_{\text{halo}} \propto M_{\text{halo}}^{-(n+3)/2}$ where n is the effective power law for the linear theory power spectrum ($P_k \propto k^n$) on the relevant scale. The rms mass fluctuation $\sigma_M \propto M_{\text{halo}}^{-(n+3)/6}$. Comparing σ_M on the scale of clusters $\sim 1.5 \times 10^{15} M_\odot$ and dwarf galaxies $\sim 2 \times 10^7 M_\odot$, for Λ CDM one obtains an effective index $n \sim -2.2$. The theory predicts a ratio of ~ 1400 for the characteristic dark matter densities of clusters and dwarfs of these scales. The observed ratio is 200, which is considerably smaller. Clearly a larger data base would be desirable, but this comparison points to a possible further problem with CDM.

IV. THE PHASE SPACE CONSTRAINT

Liouville's theorem, stating that the phase space density is conserved along particle trajectories in a collisionless fluid, provides a fundamental constraint on the clustering of warm particles [42], which we review below. Hogan and Dalcanton [17] and Sellwood [38] have recently discussed the relevance of this constraint to WDM, which unlike CDM has a finite primordial phase space density due to the thermal particle velocities. However, by the time of halo collapse the thermal particle speeds are small and have little influence on halo formation except in the very inner-most regions of massive halos [39]. The smoothing of the

primordial power spectrum which occurred at very early times, and which may be treated in linear theory as we do in the Appendix, is the main effect.

Most of the mass undergoes gravitational collapse at modest redshifts in WDM, $Z < 5$. By this time, the warm particle speeds are very low. From (10) in the Appendix, the rms speed for a 1 keV particle at $Z = 5$ would be only $v = 0.25 \text{ km s}^{-1}$, far lower than the velocities induced in gravitational collapse in any of the objects we are interested in today. Thus heating due to gravitational infall vastly outweighs the initial thermal energy, even allowing for the increase due to phase space density conservation ($v \propto \rho^{\frac{1}{3}}$).

What little remains of the primordial velocities could really only affect the far interiors of massive halo cores. To estimate this effect, let us see how the infall of warm particles into a pre-existing CDM halo would differ from CDM infall. For example, consider a particle falling into a spherical halo with density run $\rho = \rho_s(r_s/r)^2$, for $r < r_s$ (and thus a flat rotation curve). Assume for simplicity that $\rho = 0$ outside r_s . The potential energy of the particle per unit mass is $-4\pi G \rho_s r_s^2 \ln(er_s/r)$ for $r < r_s$. The principal effect of the thermal motion is to give the particle angular momentum producing a centrifugal barrier keeping the particle away from $r = 0$. This barrier is only significant for r smaller than $r_{min} \approx r_i v_{\perp} / v_{max}$ where v_{max} is the maximal radial speed induced by falling through the halo, $v_{max} \approx \sqrt{8\pi G \rho_s r_s^2 \ln(er_i/r_{min})}$, and $\langle v_{\perp}^2 \rangle = \frac{2}{3} \langle v^2 \rangle \equiv \frac{2}{3} v_{rms}^2$ is the initial thermal transverse velocity dispersion. If the halo has just virialised, the mean overdensity in r_s is ~ 150 , which implies that $\rho_s \sim 50\rho_b$ where $\rho_b = 1/(6\pi G t^2)$ is the background matter density. We should take the initial radius r_i to be a little larger than the radius of the shell now virialised at r_s when it turned around, $r_i \sim 2r_s$. Then we find $r_{min} \sim f v_{rms t}$ where t is the time when the particle turned around and f is of order $\frac{1}{10}$ divided by the square root of the logarithm. Only for radii smaller than r_{min} is the structure of the halo significantly altered relative to a pure CDM halo. For collapse at $Z = 5$, $t_c = .09 H_0^{-1}$ this gives a scale $r_{min} = 250 f h^{-1} \text{ pc}$. Generalising this calculation to other halo profiles is straightforward. For example, an NFW profile (6) yields a potential per unit mass of $-16\pi G \rho_s r_s^3 r^{-1} \ln(1 + r/r_s)$, and assuming $r_{min} \ll r_s$, one finds $v_{max} \approx \sqrt{32\pi G \rho_s r_s^2}$. The conclusions are very similar.

If we considered infall into a less symmetrical halo, we would still obtain $f < 1$. Thus it seems safe to conclude that for warm particle masses larger than 1 keV, thermal velocities are unimportant in determining the structure of halos on scales of a kiloparsec or above. They may be relevant to the formation of very small halos - if $f \sim 1$, then the mass in r_{min} is $\sim 10^5 M_{\odot}$.

In order to distinguish between the effects of reducing small-scale power and increasing thermal velocities, we have studied the collapse of massive halos numerically; an illustration is shown in Figure (3). We evolved small boxes (length $3 h^{-1} \text{ Mpc}$) of 32^3 particles, with particle masses of $6.86 \times 10^7 h^{-1} M_{\odot}$. For comparative purposes, we studied ΛCDM , and ΛWDM for $m_X = 350 \text{ eV}$, first with both the appropriate linear power spectrum and the appropriate thermal velocity distribution, and then with only the appropriate power spectrum but no thermal velocities. We do include the particle velocities from the Zeldovich approximation in the initial conditions, with the simulations starting at $Z = 40$. Identical phases were utilised for all three simulations. In the Figure, we have identified a particular object for study, which has a mass of $2 \times 10^{11} h^{-1} M_{\odot}$ (over 3000 particles). We show a phase space (r, v) plot of all the particles within a region centred on the highest density point.

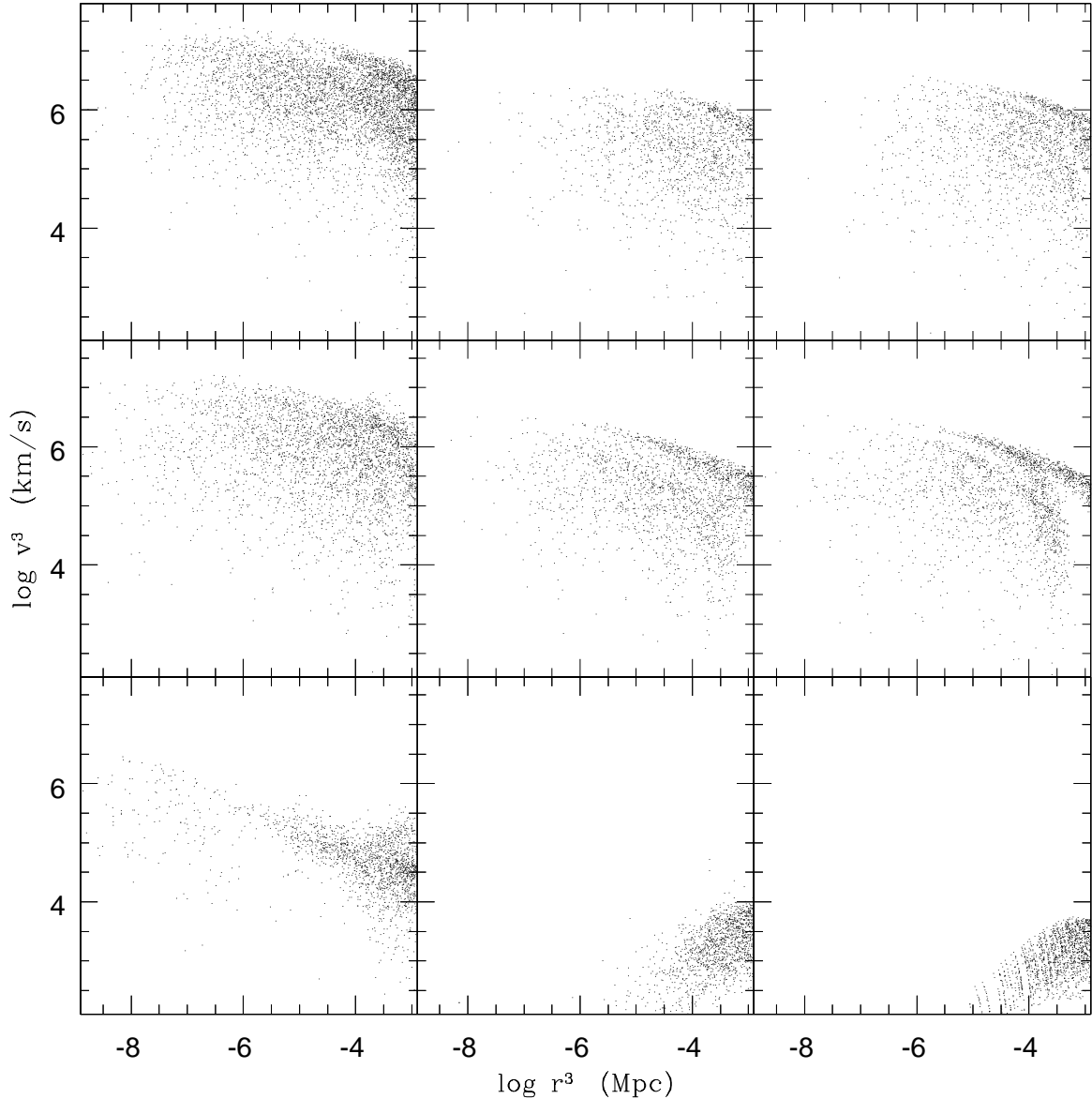


FIG. 3. The evolution of the particle distributions in phase space. A small halo of mass $2 \times 10^{11} h^{-1} M_{\odot}$ has been selected for comparative study in (left to right) Λ CDM, Λ WDM, and Λ AWDM power spectrum but without thermal velocities. From bottom to top: $Z = 8, 1$, and 0 .

The results are shown at redshifts 8, 1 and 0. In Λ CDM, the halo shows little evolution, having already begun to collapse at $Z = 8$ and relaxed to virial equilibrium well before redshift 1. The WDM halos both show substantial evolution between $Z = 8$ and 1, but not much between 1 and 0. They are very similar to each other at all redshifts, illustrating the unimportance of the initial thermal velocities on these mass scales. The value of $\rho / \langle v^3 \rangle$ near the center of this halo falls by more than four orders of magnitude over the course of the simulation.

Let us now briefly recall the bound given by Tremaine and Gunn [42] on the possible phase space density of collapsed objects. This is most relevant to the objects with highest density and lowest velocity dispersion, namely the dwarf spheroidal galaxies. Liouville's theorem states that the fine grained phase space density at the location of a fluid particle is constant in the absence of collisions. The measured phase space density can decrease due to coarse graining, but it cannot increase. For the canonical neutrino-like particle we are considering, the phase space density in the initial conditions has a maximum value of h_P^{-3} , where h_P is Planck's constant. This is the upper bound for the collapsed object. If one assumes that after virialisation the velocity distribution is Maxwellian, with one dimensional dispersion σ^2 , one obtains a final phase space density of $\rho / m_X \times (2\pi\sigma^2 m_X^2)^{-\frac{3}{2}}$. Thus the limit is

$$\rho < 2m_X^4 \left(\frac{\sqrt{2\pi}\sigma}{h_P} \right)^3. \quad (3)$$

In observational units this translates to

$$\rho < 1.6 \times 10^{-2} h^2 M_\odot \text{pc}^{-3} \left(\frac{\sigma}{\text{km s}^{-1}} \right)^3 \left(\frac{m_X}{\text{keV}} \right)^4. \quad (4)$$

With the further assumption that the core is modelled as a King profile, with core radius r_c , one finds for the central density $\rho = 9\sigma^2/(4\pi G r_c^3)$ (see e.g. ref. [13], p. 435), and thus

$$r_c > 32 \left(\frac{10 \text{ km s}^{-1}}{\sigma} \right)^{\frac{1}{2}} \left(\frac{\text{keV}}{m_X} \right)^2 \text{pc}. \quad (5)$$

Draco and Ursa Minor have core radii of ~ 200 pc and σ of 9 km s^{-1} [35], so one sees that m_X must be greater than about 400 eV for warm particles to dominate these galaxies. But this bound is weaker than others we have described above.

V. THE SIMULATIONS

Three simulations were carried out: Λ CDM and two Λ WDM models, one with warm particle mass $m_X = 350$ eV and one with 175 eV ($v_0 = 0.12$ and 0.048 km s^{-1} , respectively). The cosmological parameters are $\Omega_X = 0.3$, $\Omega_\Lambda = 0.7$, and $h = 0.67$; all models were normalized by $\sigma_8 = 0.9$ to be consistent with observations on large scales. Each simulation is a periodic cube of length $20 h^{-1} \text{ Mpc}$ containing 256^3 particles, making the particle mass $4 \times 10^7 h^{-1} M_\odot$; a Plummer softening length of $1.22 h^{-1} \text{ kpc}$ was used. The time step was set to be less than $\sqrt{0.05\epsilon/a}$ for all particles. All runs were carried out with the P³M code of Ferrell & Bertschinger [44], in the parallel version of Frederic [45].

To generate the initial conditions particles were displaced from a regular grid in the standard Z'eldovich approximation. The phases used for the displacements and velocities were identical in the three simulations. The matter power spectrum for the Λ CDM model was computed using the COSMICS package [46–48]. For WDM this was modified by the transfer function $|T_k^X|^2$ of equation (15) in the Appendix, suppressing small scale power. Warm particles were also given additional random velocities in accordance with the appropriate Fermi-Dirac distribution.

The number and distribution of virialised halos are central to our study. To locate collapsed objects the HOP code of Eisenstein & Hut [49] was used, smoothing over 32 particles when calculating the density at each point and using an outer density contour of 100 times the mean. Each halo thus identified was then considered as an isolated object, and those particles not gravitationally bound were removed. Then, using the most bound particle as the halo center, the radius r_{200} of the sphere enclosing a mean overdensity of 200 was found, as well as the mass M_{200} inside this radius. Objects with $M_{200} < 10^9 h^{-1} M_\odot$, i.e. with fewer than 25 bound particles, are removed from further consideration.

These simulations do not have the resolution required to go to the smallest observational scales, since we only resolve objects $\gtrsim h^{-1} 10^9 M_\odot$. A second limitation is that the runs become computationally costly at low redshifts. Hence we shall show results for these large boxes only down to redshift unity. We have performed smaller (128^3 particles with $3h^{-1}$ box size) simulations to redshift zero, for a more realistic warm particle mass of 1.5 keV, which we also discuss below.

VI. EVOLUTION AND CLUSTERING PATTERN

Figure (4) shows the projected density in three runs of Λ CDM and Λ WDM with warm particle masses of 175 and 350 eV. From top to bottom, the boxes are shown at redshifts Z of 3, 2 and 1. The most obvious distinction is that the warm boxes have less structure at $Z = 3$, especially on small scales. This illustrates the constraint posed by the requirement of early galaxy and quasar formation in a WDM cosmology, and of course the requirement that the universe be re-ionised at least by $Z \sim 5$.

The second feature of the figure is that the clustering pattern on large scales is identical in the three cases, as is to be expected given the identical phases used to generate the initial conditions. However on smaller scales interesting details are revealed. In the Λ CDM model the regions between the ‘cosmic web’ structure are filled with small halos, which do not occur at all in the warm models. Small halos are formed in the warm models, but only within the caustic surfaces (‘ribbons’) of the ‘cosmic web’. The different clustering patterns are shown in more detail in Figure (5), where the spatial distribution of halos of three mass ranges are plotted. In the CDM model the small halos $M < 9 \times 10^9 h^{-1} M_\odot$ fill the voids, whereas in the warm models they closely trace a ‘cosmic web’ pattern of remarkably thin (and cold) caustic sheets.

An illustration of the typical environment of a halo is shown in Figure (6). Here the local density around each halo is calculated by measuring the total mass within a $1 h^{-1}$ Mpc sphere surrounding the halo center. The cumulative fraction of halos as a function of the local density is plotted. The plot shows that half of the less massive halos (10^9 to $9 \times 10^9 h^{-1} M_\odot$) in the cold model are located in low density regions at less than twice the

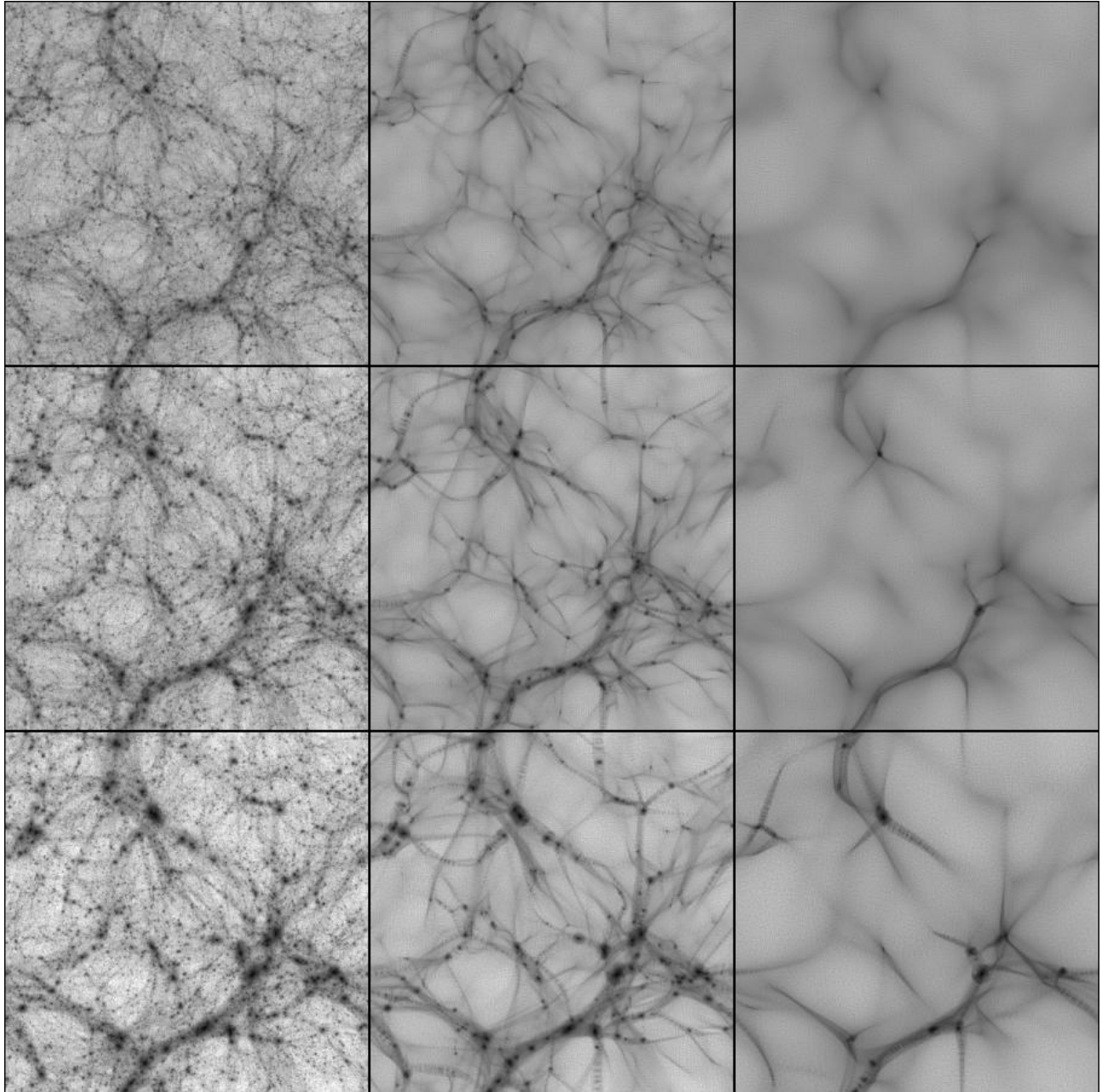


FIG. 4. Projected density of $20 h^{-1}\text{Mpc}$ boxes, on a logarithmic scale of surface density. Left to right: ΛCDM , $m_X = 350 \text{ eV}$ and $m_X = 175 \text{ eV}$ AWDM. Top to bottom: redshift $Z = 3, 2$, and 1 . A higher resolution version of this Figure is available at the web site referred to in the introduction. A simulation with $m_X > 1 \text{ keV}$ would have an appearance intermediate between the left and central columns.

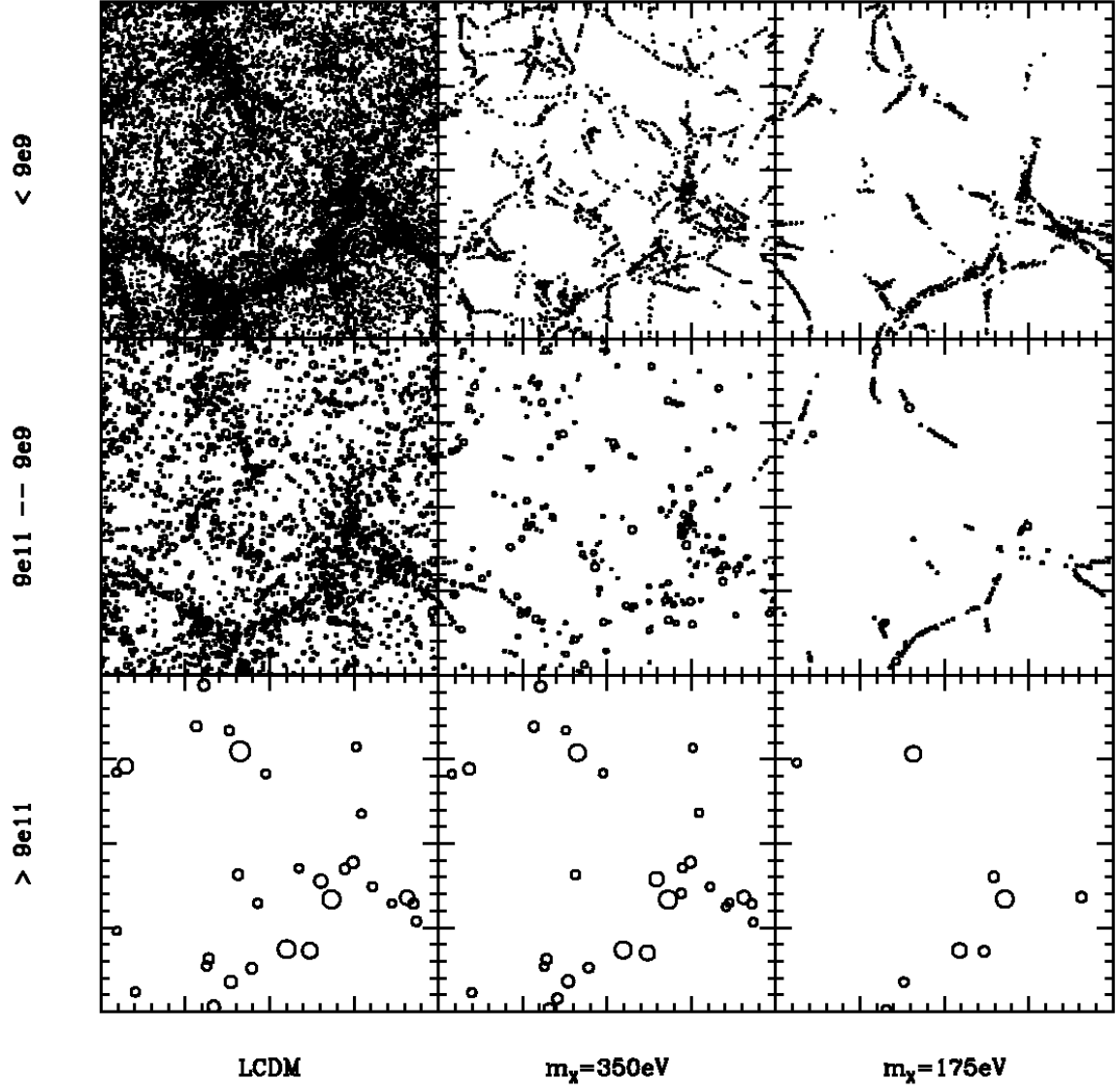


FIG. 5. Position of gravitationally bound halos at redshift $Z = 1$, corresponding to the top row of Figure (4). Bottom to top: high ($M_{200} > 9 \times 10^9 h^{-1} M_\odot$), intermediate ($9 \times 10^9 h^{-1} M_\odot < M_{200} < 9 \times 10^{11} h^{-1} M_\odot$), and low mass ($9 \times 10^{11} h^{-1} M_\odot < M_{200} < 10^9 h^{-1} M_\odot$) halos. Left to right: Λ CDM, $m_X = 350$ eV and $m_X = 175$ AWDM. The radius of each circle is r_{200} . In WDM, the formation of low mass objects is in ribbon-like structures connecting higher mass halos. Note the almost complete absence of small halos outside these regions, while the highest mass halos (bottom row) are quite similar to LCDM.

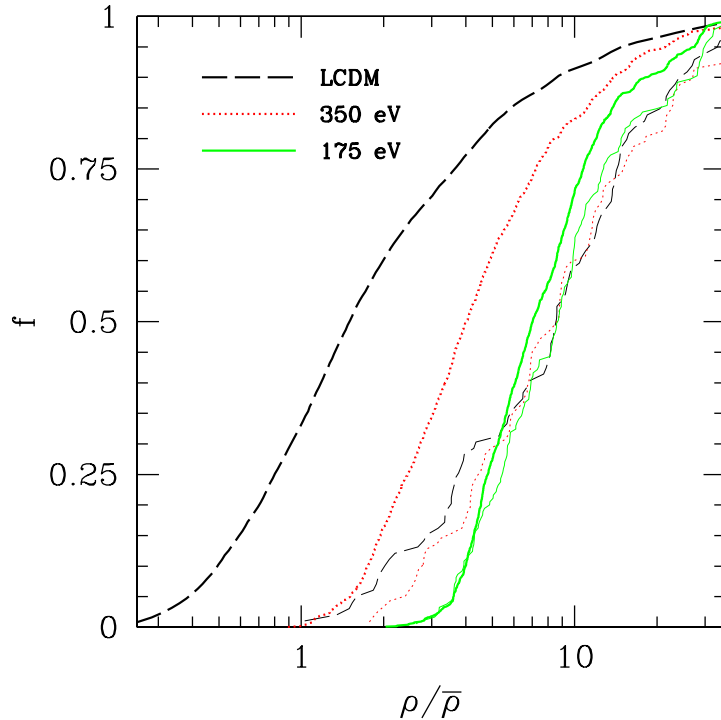


FIG. 6. The mass density in the vicinity of halos. The plot shows the cumulative fraction of halos as a function of the mean density in a $1 h^{-1}$ Mpc radius sphere centered on the halo. Thick lines are for halos with mass $(9 \times 10^9 > M > 10^9 h^{-1} M_\odot)$, thin ones for only mass greater than $10^{12} h^{-1} M_\odot$. One sees that the WDM models have far fewer halos in low density neighbourhoods: they form instead in higher density caustics. For high mass halos the differences in environment are relatively small.

mean density. In the warm models, almost all such halos are in regions denser than this. The median local overdensity increases from 1.5 for CDM to 4 and 7 for 350 and 175 eV WDM respectively. Results for larger halos only ($> 10^{12} M_\odot$) are also plotted, revealing little difference in their mean environments between the three models. In the 175 eV model, the distribution for larger halos is quite similar to that for small halos, showing that smaller halos form in the same filamentary environment.

A blow-up of one octant of each cube is shown in Figure (7). The suppression of small scale structure in the warm models is evident. The closer view of massive halos reveals many satellite halos in the ΛCDM model, but very few in the warm models. This is quantified statistically in Figure (8), which shows the average number of satellite halos within each halo. This number defined by measuring the distances separating each pair of halos: if this distance is smaller than the sum of their radii (defined as the radius enclosing mean overdensity 200), then the less massive halo is counted as a satellite of the more massive halo. There is strong suppression of the number of satellites of the massive halos in WDM, by roughly a factor of 5. Somewhat surprising is that the effect is even larger for the 350 eV warm particles than for the 175 eV particles. The number depends on both the rate at which satellites are accreted and the rate at which they are tidally destroyed [21]. In WDM small halos are found in denser regions; on the other hand, having formed later these are

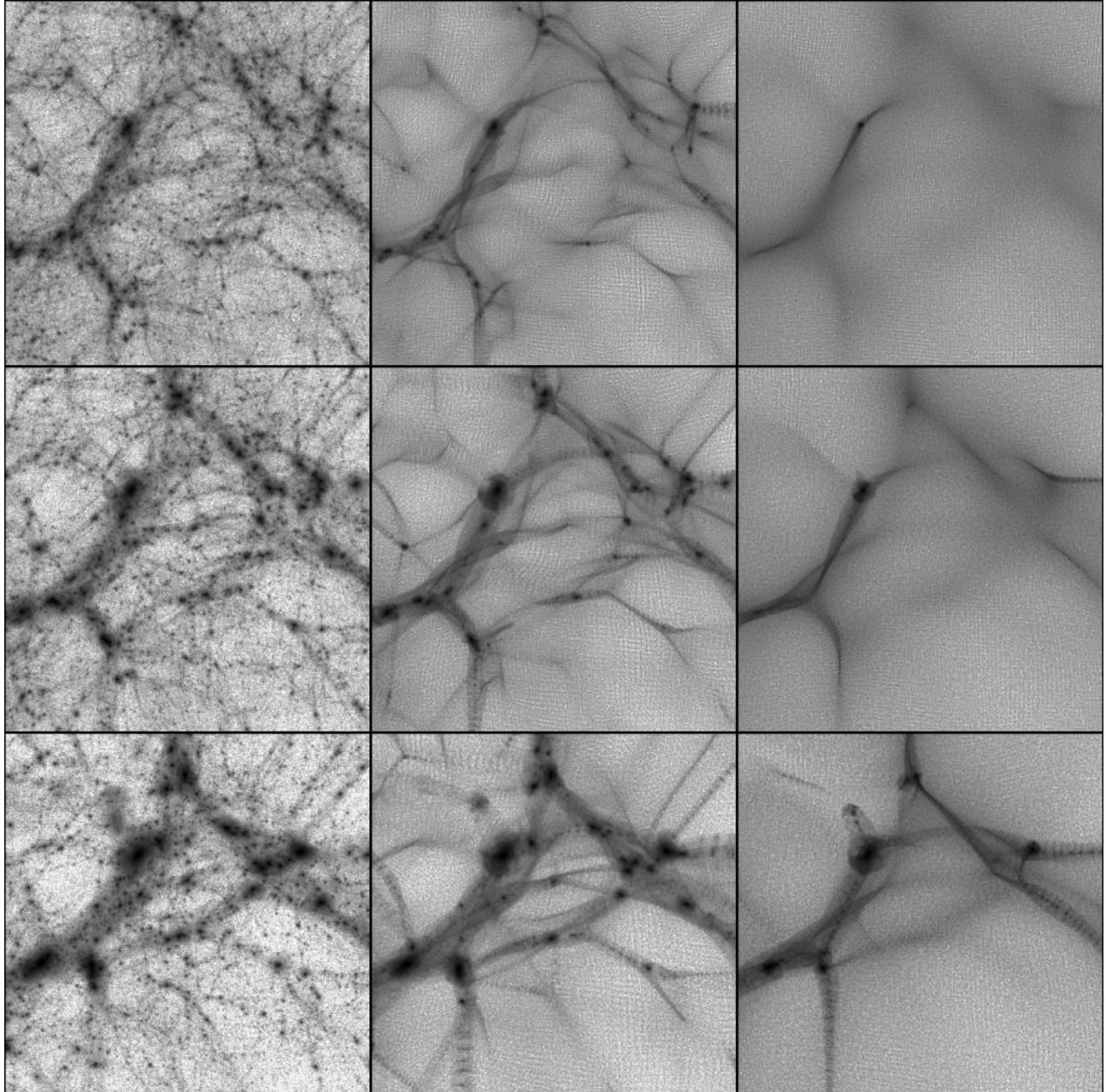


FIG. 7. Projected density in one octant of the $20h^{-1}$ Mpc cubes shown above. The small scale structure present in the CDM model is clearly visible, as is the relative suppression of satellite galaxies about the larger halos in the warm models. A higher resolution version of this Figure is available at the web site referred to in the introduction.

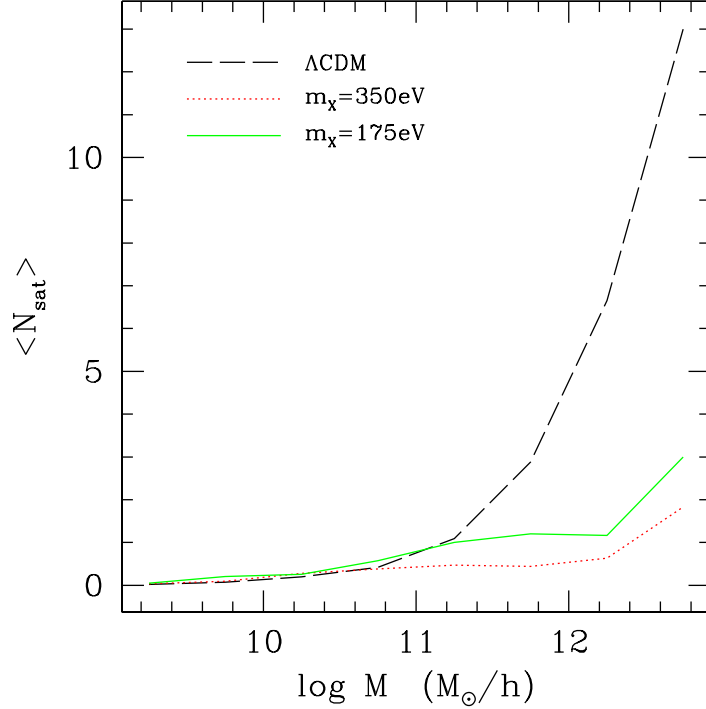


FIG. 8. Average number of satellites, as a function of the mass of the parent halo. See text for method of satellite identification.

less dense and thus more easily disrupted when encountering a massive halo.

Careful examination of the web structures in the central column reveals at late times a fairly regular pattern of instability with wavelength of maximum growth being comparable to the transverse ribbon dimension. We believe this fragmentation pattern is a real reflection of the top down instability.

To summarise the findings of this section, we see that the bulk of the low mass halos are formed in the classic ‘top down’ structure formation scenario, via the fragmentation of large ribbons and pancakes. However we see this taking place on relatively small scales, within a scenario in which hierarchical ‘bottom-up’ structure formation is simultaneously occurring on larger scales.

In the next section we quantify the abundances and properties of halos in the three simulations.

VII. HALO ABUNDANCES AND STRUCTURE

Figure (9) shows the halo mass function found in the three models. There are two features distinguishing the Λ WDM models from Λ CDM. First, there is a strong suppression of low mass halos, consistent with the cutoff seen in the linear power spectrum. This suppression is seen for masses below the scale set by equation (1), $\frac{4}{3}\pi\rho_b R_S^3$, or 4×10^{11} and $4 \times 10^{12}h^{-1}M_\odot$ for $m_X = 350$ and 175 eV respectively. Secondly, the mass function becomes much steeper again at the lowest masses. However, these low mass halos are not formed early, as the corresponding cold dark matter halos are. Rather they are formed via pancake

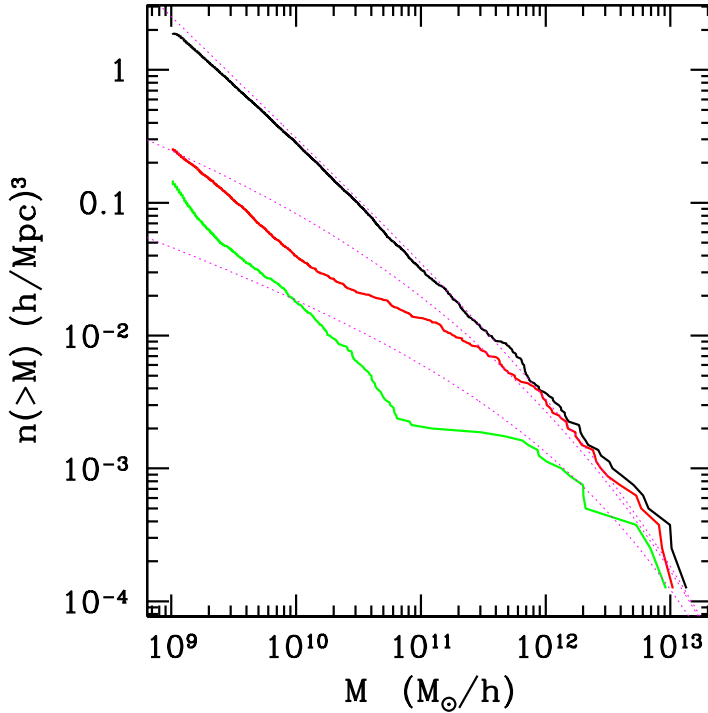


FIG. 9. Number density of halos of each mass for three models (thick lines). Top to bottom: Λ CDM, $m_X = 350\text{eV}$ ($v_0 = 0.048 \text{ km s}^{-1}$) and $m_X = 175\text{eV}$ ($v_0 = 0.12 \text{ km s}^{-1}$) Λ WDM. The thin dashed lines are predictions from the formula of Sheth, Mo, & Tormen (1999).

fragmentation as explained above, and therefore at lower redshifts and with correspondingly low densities.

Sheth, Mo, & Tormen [51] improved on the standard Press-Schechter excursion set approach to provide a prediction of the abundances of collapsed dark matter halos (the approach of Jenkins et al. [52] gives quite similar results). We compare this prediction with the numerical results in Figure (9). Λ CDM is fit very well across the entire mass range of the simulation. For the WDM models, which have a strong maximum in the power spectrum within the wavenumber range involved in nonlinear clustering, the excursion set approach fits poorly on scales below that set by the smoothing length R_S . The rms mass fluctuation σ on scales relevant to small masses is roughly constant, as is shown in Figure (2). Thus the effective spectral slope is highly negative, and well outside the parameter space in which the analytic formulas have been tested (see Figure (9) of Jenkins et al. [52]). These formulae also do not predict an upturn at smaller scales, which is hardly surprising, since the formation of the small halos occurs via caustic fragmentation, and has very little to do with the initial power spectrum smoothed on the appropriate comoving mass scale.

The density profiles of each halo were fit to a NFW profile [53]

$$\rho(r) = \frac{4\rho_s r_s^3}{r(r + r_s)^2}, \quad (6)$$

which is a convenient parameterization. The core size r_s measures roughly the point where the rotation curve of such a halo should flatten, and ρ_s is the value of the density at that

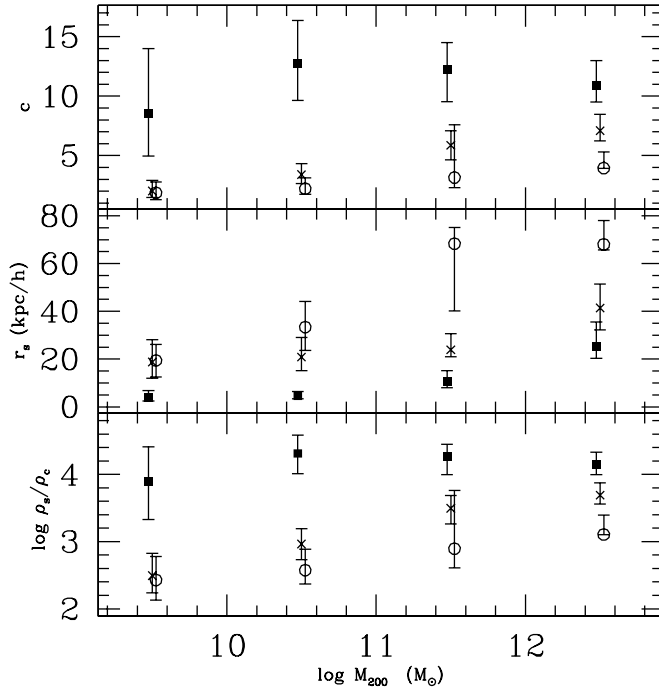


FIG. 10. Mean values for the NFW concentration parameter $c = r_{200}/r_s$, core radius and core density (defined in equation 6) as a function of mass M_{200} . *Filled squares*: LCDM. *Crosses*: $m_X = 350\text{keV}$ ($v_0 = 0.048 \text{ km s}^{-1}$) WDM. *Circles*: $m_X = 175\text{keV}$ ($v_0 = 0.12 \text{ km s}^{-1}$) WDM.

radius, which we term the ‘characteristic’ density. This was done by computing the density in radial bins of width $3 h^{-1}\text{kpc}$ and finding the best-fit parameters $c = r_{200}/r_s$ and r_s by minimizing χ^2 ; if the reduced χ^2 gave less than a 90% probability for the fit then that halo was not used in the following analysis.

Figure (10) shows the resulting concentration parameter c , r_s , and ρ_s as a function of halo mass for each of the models studied. For the lowest masses the differences are quite substantial. The WDM halos show lower densities and central concentrations than the corresponding cold dark matter ones. Thus the WDM halos are in better agreement with observations of nearby dwarf galaxies than standard CDM [54]. While smaller, these differences persist up to higher mass halos formed in the normal (bottom up) fashion. In the normal CDM model the central parts of high-mass halos are from accreted low-mass, high-density halos [11]; in WDM such accreted objects are rare. Colin, Avila-Reese & Valenzuela [21], using a warm particle mass of 604 or 1017 eV, found that lower-mass satellites found around Milky-Way sized halos have concentration factors lower by a factor of 2 compared to Λ CDM. This appears to be in good agreement with Figure (10).

VIII. A HIGHER WARM PARTICLE MASS M_X

The WDM simulations discussed above are for particle masses too low to reconcile with the limits discussed in Section I, which indicate $m_X \gtrsim 1 \text{ keV}$. While they are useful for identifying qualitative trends, one may ask if the differences with standard CDM discussed

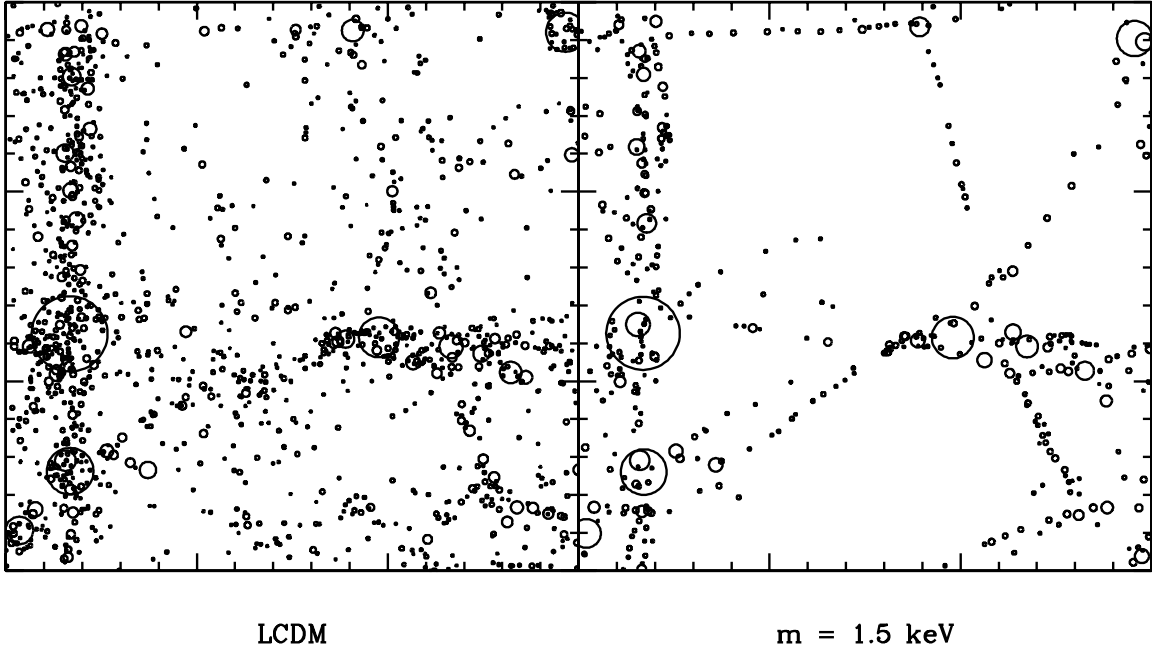


FIG. 11. Position of gravitationally bound halos at redshift $Z = 0$ in a $3 h^{-1}\text{Mpc}$ box, for ΛCDM (left) and ΛWDM with $m_X = 1.5 \text{ keV}$ (right). The radius of each circle is r_{200} . The smallest halo mass is $2.7 \times 10^7 h^{-1} M_\odot$. Finite box size effects are visible in the orientation of the largest pancake, but it is clear that the environment of small halos is distinct between the two scenarios.

above persist to higher particle masses. To test this, an additional pair of simulations were made; one was ΛCDM with the same cosmological parameters as before, and the other was ΛWDM with $m_X = 1.5 \text{ keV}$. The box size was chosen to be $3 h^{-1}\text{Mpc}$, with $N = 128^3$ particles. These runs were carried out and analysed in the same manner as described in Section 5; because of the smaller number of particles they could be evolved to redshift zero. For such a small box, it is inevitable that there are sizeable finite size effects, and these are visible in the orientation of the largest pancake.

The trends seen for lower warm particle masses are also present in this 1.5 keV run. Figure (11) shows the positions of halos identified in the two simulations; shown are halos with bound masses larger than $2.7 \times 10^7 h^{-1} M_\odot$ (25 particles). The number of low mass halos is suppressed in the WDM model by a factor of over three, and it can be seen that small halos trace the caustic structures connecting the largest ones. This is in contrast with small CDM halos, which occur in voids as well. The WDM halos tend to be found in denser environments as well. Using a sphere of $300 h^{-1}\text{kpc}$ to define the local overdensity, only 20% of the WDM halos are in regions with local overdensity less than unity, while 40% of the CDM halos are. The larger WDM halos have fewer satellites: only 17 satellites are found around the ten largest WDM halos (with masses $\gtrsim 10^{10} h^{-1} M_\odot$), while the ten largest CDM halos have 97. The WDM halo profiles are also quite distinct from CDM. Fitting with the NFW profile, the mean concentration parameter is lower by a factor of 2.5, and the mean core radius is larger by a factor of 3. The overdensity at r_s has mean $\sim 2 \times 10^5$ in ΛCDM

with a few halos above 10^6 ; in WDM the mean is $\sim 2 \times 10^4$ with $\sim 10^5$ as the maximum.

There is definitely room for more detailed study, but this pair of runs indicates that the trends described in our larger runs do persist as the warm particle mass is increased.

IX. CONCLUSIONS

We have identified several key observational features of WDM clustering which serve to distinguish it from cold dark matter. The principal difference is due to the ‘top down’ formation of structure below a characteristic mass scale, which we can roughly quantify as

$$M_S = 1.0 \times 10^{10} \left(\frac{\Omega_X}{.3} \right)^{1.45} \left(\frac{h}{.65} \right)^{3.9} \left(\frac{\text{keV}}{m_X} \right)^{3.45} h^{-1} M_\odot. \quad (7)$$

Below this mass scale, objects are formed primarily by the fragmentation of pancakes and ribbons. They are rarer and considerably less dense than halos of the same mass in CDM. And their spatial distribution is very different - they are concentrated in sheets and ribbons running between the massive halos, an effect which has been noted for some time for dwarf galaxies in the local universe [12]. Finally, the dwarf galaxies form later than bright galaxies, contrary to the hierarchical picture of clustering in CDM theory. Again WDM seems to be in better agreement with the observations on this point [14].

This work points to the need for the following observational tests to verify or refute the predicted signatures, namely:

- Observations revealing the ionisation history and Lyman α cloud distribution at redshifts higher than 6.
- Observations revealing the history of galaxy formation and checking whether low mass galaxies formed later than higher mass galaxies, as in WDM, or earlier as in CDM.
- Determination of the abundance, masses, density profiles and clustering pattern of dwarf galaxies relative to large galaxies. A recent study [55] indicates that the dwarf to giant ratio increases with increasing density, consistent with our findings here. Likewise the apparent absence of dwarf systems in the voids noted by Peebles [12] needs to be carefully quantified and compared with CDM and WDM simulations.
- High accuracy observations measuring the inner parts of galaxy rotation curves and comparing them with detailed N body simulations of Λ WDM and Λ CDM.
- Observations of the abundances of satellites in galaxies other than the Milky way. Especially important is a determination of the characteristic densities of dwarf dark matter dominated systems, as compared to dwarf halos in simulations.

It is clear that a great deal also needs to be done in simulating WDM, to better quantify the qualitative features we have noted here. This will require higher resolution codes and considerable amounts of computation time.

Acknowledgements

We would like to thank R. Battye, G. Efstathiou, R. Lopez, J. Peebles, M. Rees, and P. Steinhardt for useful discussions. Special thanks are owed to C-P. Ma who kindly provided Boltzmann code results.

This research was supported by NSF Grant AST-9803137 (under Subgrant 99-184), and the NCSA Grand Challenge Computation Cosmology Partnership under NSF Cooperative Agreement ACI-9619019, PACI Subaward 766. The work of NT was supported by a PPARC (UK) rolling grant, and PPARC and HEFCE (UK) grants to the COSMOS facility. NT thanks the ITP (Santa Barbara) for hospitality while this paper was being completed.

X. APPENDIX: LINEAR THEORY

In this appendix we review the standard results concerning thermal relic warm dark matter and then discuss a simplified approach to understanding damping by free streaming, which illustrates the physics and tells us how the power spectrum should scale as the mass of the warm particle, and the cosmological parameters are varied. We explain the calculation of the smoothing length R_S given in equation (1) above.

For a thermal relic X which decouples when relativistic, the abundance relative to photons is

$$\frac{n_X}{n_\gamma} = \frac{\frac{43}{11}}{g_{dec}} \frac{g_X}{1.5} \quad (8)$$

where g_{dec} is the effective number of relativistic species present at X decoupling. Bosonic spin degrees of freedom contribute unity and fermionic ones $\frac{3}{4}$. A light neutrino contributes $g_X = 1.5$, and we shall usually assume this holds for the warm particle. The dependence in (8) comes about because annihilation degrees of freedom after X decoupling heats the photons but not the X 's.

The abundance of X 's fixes their density through $\rho_X = m_X n_X$. This yields

$$\Omega_X h^2 \approx \frac{115}{g_{dec}} \frac{g_X}{1.5} \frac{m_X}{\text{keV}}. \quad (9)$$

As mentioned in Section 2, if entropy producing processes occur subsequent to X decoupling, they act in a manner as to mimic an increase in g_{dec} .

The second quantity of interest is the velocity dispersion of the X particles, since this is what causes the smearing of small scale primordial perturbations. If the X particles decouple when relativistic, the distribution function $(e^{(p/T_X)} + 1)^{-1}$ remains constant until gravitational clustering begins. All particle momenta scale as a^{-1} which we can describe by scaling T_X accordingly. When the particles become non-relativistic we can use $p = m_X v$, with v their speed. The distribution function is then $(e^{(v/v_0)} + 1)^{-1}$, with

$$v_0(Z) \approx .012 (1 + Z) \left(\frac{\Omega_X}{.3} \right)^{\frac{1}{3}} \left(\frac{h}{.65} \right)^{\frac{2}{3}} \left(\frac{1.5}{g_X} \right)^{\frac{1}{3}} \left(\frac{\text{keV}}{m_X} \right)^{\frac{4}{3}} \text{km s}^{-1}, \quad (10)$$

at redshift Z . The *rms* velocity is $\sqrt{4\pi}v_0$.

A crude estimate of the free streaming lengthscale is obtained by calculating the comoving distance a particle moves after matter-radiation equality. This is proportional to (10) evaluated at $Z_{eq} = 2.39 \times 10^4 \Omega_M h^2$, times the comoving horizon scale at that time, $16.0/(\Omega_M h^2)$ Mpc (for three light neutrinos). Thus one obtains the scaling given in (2), from references [18], [19]. As mentioned in the introduction however this scaling is incorrect due to additional streaming in the radiation era, as we shall now discuss.

For the masses m_X we discuss here, most of the smoothing of the initial perturbations occurs when the particles are nonrelativistic. The free streaming may then be understood via an analytic solution of the Gilbert equation obtained by treating the background radiation as uniform, and making a certain approximation to the Fermi-Dirac distribution [56]. This approximation is useful for revealing the main parameter dependence of the transfer function.

The perturbation in each plane wave mode of X is governed by Gilbert's equation (for a derivation see [56])

$$\delta_{X,\mathbf{k}}(z) = \delta_{X,\mathbf{k}}^{nog}(z, z_0) + 6 \int_{z_0}^z dz' \delta_{X,\mathbf{k}}(z') \frac{F(z, z')}{[1 + A^2 F(z, z')]^2} \quad (11)$$

where $\delta_{X,\mathbf{k}}^{nog}(z, z_0)$ is a solution to the free streaming equation in the absence of self-gravity. $F(z, z') = \ln(1 + z'^{-1}) - \ln(1 + z^{-1})$, where $z = \tau/(4\tau_*)$, and τ is the conformal time. The scale factor is chosen to be unity at matter-radiation equality, and is given by $a = 4(z + z^2)$ [56] (Note that z is not the redshift). In (11), the quantity $A = k\tau_* v_0(Z_{eq})$ where k is the comoving wavenumber, and the comoving value of the scale $(1 + Z_{eq})\tau_* = 19.4\Omega_M^{-1}h^{-2}$. The comoving horizon scale given earlier is $2(\sqrt{2} - 1)$ times this scale. Finally, $v_0(Z_{eq})$ is given in equation (10).

Equation (11) is derived by approximating the distribution function $(e^{\frac{p}{T}} + 1)^{-1}$ as $e^{-\frac{p}{T}}$ times an appropriate normalisation factor [56]. In this approximation bosons and fermions behave identically.

Equation (11) shows the scale $\tau_* v_0(Z_{eq})$ entering, in comoving units. This is the speed of the warm particles times the horizon at matter-radiation equality. This leads to the estimate of $R_{>eq}$ in (2). However, the Gilbert equation requires initial conditions, and specification of the non-gravitating solution $\delta_{X,\mathbf{k}}^{nog}(z, z_0)$. This is where additional parameter dependence enters. The point is that no growth of perturbations occurs whilst the X particles are relativistic, because the Jeans length is of order the horizon scale. When the X particles slow down, the Jeans length starts increasing, reaches its maximum, and thereafter decreases. The Gilbert equation only applies after the maximum Jeans length is attained, which is when the X 's become nonrelativistic. The X particles' rms speed falls to $\sim 0.3c$ when z becomes greater than

$$z_0 \approx .02 (\Omega h^2 / m_X)^{\frac{4}{3}} (1.5 / g_X)^{\frac{1}{3}}, \quad (12)$$

which we adopt as the initial value in the Gilbert equation. Note that this combination of parameters differs from that entering $R_{>eq}$ in (2).

The free streaming solution $\delta_{X,\mathbf{k}}^{nog}(z, z_0)$ should be calculated using the full relativistic equations, by integrating the perturbations across horizon crossing. However, no additional cosmological parameter dependence enters this phase since it is deep in the radiation era. If we are only interested in the suppression of structure relative to that in cold dark matter, it

is reasonable to take a simple isotropic ansatz (i.e. a perturbation of the local temperature) for $\delta_{X,\mathbf{k}}^{nog}(z, z_0)$ and then compare its evolution with that predicted from the same equation for the $k = 0$ mode, which is unaffected by streaming. In the same approximations as used above, we find

$$\delta_{X,\mathbf{k}}^{nog}(z, z_0) \propto \frac{1 - \frac{1}{3}A^2 F(z, z_0)^2}{(1 + A^2 F(z, z_0)^2)^3}. \quad (13)$$

With the source fully specified, equation (11) is easily iterated numerically into the matter era where the amplitude of the growing mode density perturbation is compared to that for $k = 0$ to obtain the transfer function.

The smoothing kernel depends on the smoothing scale $R_{>eq}$ in (2), and z_0 in (12). Dimensional analysis then yields a smoothing scale $R_{>eq} f(x)$ with $f(x)$ an arbitrary function and $x = (\Omega h^2/m_X)^4 (1.5/g_X)$. The results of the Gilbert equation code are well fitted by

$$T_k^X = (1 + (\alpha k)^2)^{-5} \quad (14)$$

with $\alpha = 0.05 (\Omega_X/0.4)^{1.15} (h/0.65)^{1.3} (\text{keV}/m_X)^{1.15}$ and k in $h \text{ Mpc}^{-1}$, i.e. $f(x) = 0.05 x^\beta$ and $\beta \approx -0.18$. This additional dependence, which weakens the decrease of smoothing length as m_X is increased, is due to the fact that higher mass particles become non-relativistic sooner and therefore go through a longer period of free streaming in the radiation era.

A full Boltzmann code calculation [57], yields a fit

$$T_k^X = (1 + (\alpha k)^{2\nu})^{-5/\nu} \quad (15)$$

with

$$\alpha = 0.048 (\Omega_X/0.4)^{1.15} (h/0.65)^{1.3} (\text{keV}/m_X)^{1.15}, \quad (16)$$

and $\nu = 1.2$, which is accurate to a few per cent over the relevant range of k . The scaling, and the fitting function, are illustrated in Figure (12). The warm dark matter power spectrum to be input into N body simulations is then given by that for cold dark matter multiplied by $|T_k^X|^2$. The particle velocity distribution is given in (10).

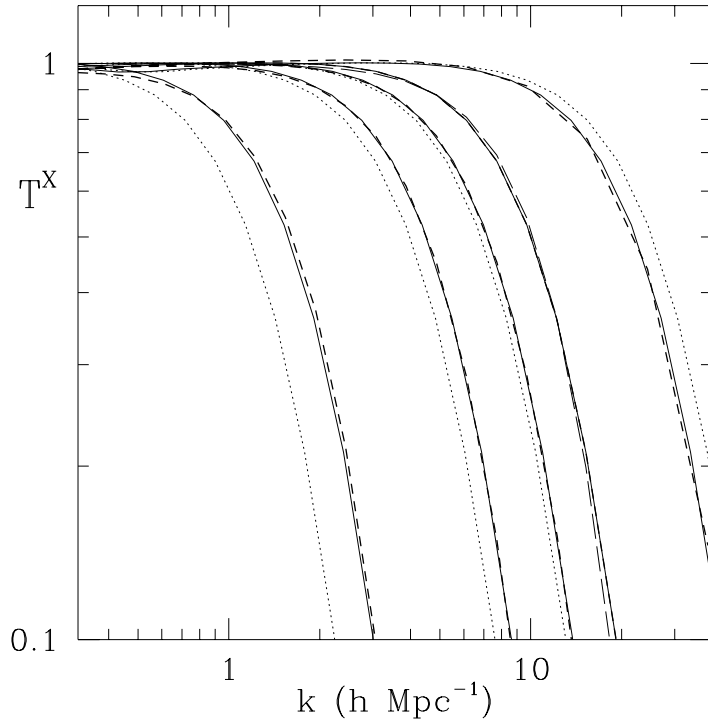


FIG. 12. The transfer function $T_k^X \equiv \sqrt{P_k^X/P_k^{CDM}}$ as computed with an accurate Boltzmann code [55], for $m_X = 0.2, 0.5, 0.75, 1.0$ and 2.0 keV, (bold dashed curves, left to right). The 1 keV curve is then re-plotted after rescaling k by $m_X^{1.15}$, for each mass, as solid lines. The same curve is also re-plotted after the rescaling of $m_X^{4/3}$, as dotted lines, demonstrating that this scaling is incorrect. The fit we have adopted in equation (15) is shown as a long-dashed curve.

REFERENCES

- [1] B. Moore, S. Ghigna, F. Governato, G. Lake, T. Quinn, J. Stadel and P. Tozzi, astro-ph/9907411, Ap. J. Lett., submitted (1999); S. Ghigna *et al*, astro-ph/9910166, Ap. J., submitted (1999).
- [2] M. Mateo, Annual Reviews of Astronomy and Astrophysics; Vol 36, 435 (1998), astro-ph/9810070.
- [3] B. Moore, T. Quinn, F. Governato, J. Stadel and G. Lake, astro-ph/9903164, MNRAS submitted (1999).
- [4] J. Sommer-Larsen and A. Dolgov, astro-ph/9912166, submitted to Ap. J. (1999).
- [5] J.F. Navarro and M. Steinmetz, astro-ph/0001003, Ap. J., submitted (2000).
- [6] J.S. Bullock, A.V. Kravtsov, D.H. Weinberg, astro-ph/0002214.
- [7] J. Binney, O. Gerhard, J. Silk, astro-ph/0003199.
- [8] M. Irwin and D. Hatzidimitriou, M.N.R.A.S, **277**, 1354 (1995).
- [9] F. C. van den Bosch, R. A. Swaters, astro-ph/0006048, submitted to AJ; R. A. Swaters, astro-ph/0009370.
- [10] A. Klypin, A.V. Kravtsov, J. Bullock and J. Primack, astro-ph/0006343.
- [11] Subramanian, K., Cen, R. & Ostriker, J.P. 2000, ApJ, 538, 528.
- [12] P.J.E. Peebles, in Clustering at High Redshift, ed. A. Mazure, O. Le Fevre, & V. Le Brun (San Francisco: Astronomical Society of the Pacific) 2000.
- [13] P.J.E. Peebles, *Principles of Physical Cosmology*, Princeton University Press, 1993.
- [14] N. Metcalfe, T. Shanks, A. Campos, H.J. McCracken and R. Fong, astro-ph/0010153.
- [15] Bahcall, N.A., Ostriker, J.P., Perlmutter, S., & Steinhardt, P.J. 1999, Science, 284, 1481
- [16] S. Colombi, S. Dodelson and L.M. Widrow, astro-ph/9505029.
- [17] C. J. Hogan and J.J. Dalcanton, Phys.Rev. D62 (2000) 063511, astro-ph/0002330.
- [18] J.R. Bond and A. Szalay, Ap. J. **274**, 443 (1984).
- [19] J.M. Bardeen, J.R. Bond, N. Kaiser and A.S. Szalay, Ap. J. **304**, 15 (1986).
- [20] V. K. Narayanan, D. N. Spergel, R. Dave, C-P. Ma, astro-ph/0005095, Ap. J. Lett. submitted (2000).
- [21] P. Colin, V. Avila-Reese and O. Valenzuela, astro-ph/0004115, ApJ, in press (2000).
- [22] P. Colin, V. Avila-Reese and O. Valenzuela, astro-ph/0009317.
- [23] M. White & R.A.C. Croft, astro-ph/0001247.
- [24] M. Kawasaki, N. Sugiyama and T. Yanagida, hep-ph/9607273, Mod. Phys. Lett. **A12**, 1275 (1997).
- [25] M. Kawasaki, K. Kohri and N. Sugiyama, astro-ph/0002127.
- [26] G. F. Giudice, E.W. Kolb and A. Riotto, hep-ph/0005123.
- [27] Unfortunately refs. [25] and [26] are apparently inconsistent in their neutrino densities by over an order of magnitude. We understand the origin of the discrepancy is still unclear (G. Giudice, private communication).
- [28] S. Thomas, hep-ph/9506274, Phys.Lett. B356 (1995) 256.
- [29] A. Dolgov and S.H. Hansen, hep-ph/0009083.
- [30] W.B. Lin, D.H. Huang, X. Zhang, R. Brandenberger, astro-ph/0009003.
- [31] J.E. Gunn and B.A. Peterson, Ap. J. **142**, 1633 (1965).
- [32] V.R. Eke, S. Cole and C.S. Frenk, 1996, MNRAS 282 263
- [33] Gnedin, N.Y. & Ostriker, J.P. 1997, ApJ 486 581

[34] Barkana R., Haiman, Z., & Ostriker, J.P. 2001, in preparation

[35] S. van den Bergh, The Galaxies of the Local Group, Cambridge University Press, 2000.

[36] K. Rines, M.J. Geller, A. Diaferio, J.J. Mohr and G.A. Wegner, astro-ph/0007126.

[37] P. Madau, astro-ph/0003096, Phil. Trans. R. Soc. London A (2000) 358.

[38] J. A. Sellwood, astro-ph/0004352, Ap. J. Lett. **i540**, L1 (2000).

[39] Sellwood's conclusion that WDM is ruled out by the observed variation in phase space densities for galaxies does not apply to warm particle masses greater than ~ 100 eV. We thank him for this clarification.

[40] D. Stern *et al.*, astro-ph/0002338, Ap. J. Lett., to appear (2000).

[41] X. Fan *et al.*, astro-ph/0005414, Ap. J., to appear (2001).

[42] S. Tremaine and J.E. Gunn, Phys. Rev. Lett. **42**, 407 (1979).

[43] J.J. Dalcanton and C. J. Hogan, astro-ph/0004381, Ap. J. submitted (2000).

[44] Ferrell, R. & Bertschinger, E. 1994, Int. J. Mod. Phys. C, 5, 933.

[45] Frederic, J.J. 1997, Ph.D. Thesis, MIT.

[46] Bertschinger, E. 1995, astro-ph/9506070.

[47] Ma, C. & Bertschinger, E. 1995, ApJ, 455, 7.

[48] Bode, P.W., & Bertschinger, E. 1995, Supercomputing '95, IEEE Computer Society, 1995.

[49] Eisenstein, D.J. & Hut, P. 1998, ApJ, 498, 137.

[50] R.S. Somerville, G. Lemson, T.S. Kolatt, and A. Dekel, MNRAS, 2000 in press, astro-ph/9807277.

[51] R.K. Sheth, H.J. Mo, & G. Tormen 1999, MNRAS, submitted, astro-ph/9907024.

[52] Jenkins, A., Frenk, C.S., White, S.D.M., Colberg, J.M., Cole, S., Evrard, A.E. & Yoshida, N. 2000, MNRAS, in press (astro-ph/0005260).

[53] Navarro, J.F., Frenk, C.S. & White, S.D.M. 1997, ApJ, 490, 493

[54] F.C. van den Bosch, B.E. Robertson, J.J. Dalcanton & W.J.G de Blok 1999, astro-ph/9911372.

[55] A.I. Zabludoff and J.S. Mulchaey, Ap. J., **539**, 136 (2000).

[56] R. Brandenberger, N. Kaiser and N. Turok, Phys. Rev. **D 36**, 2242 (1987).

[57] C.-P. Ma, private communication.